RSC Advances

This is an *Accepted Manuscript*, which has been through the Royal Society of Chemistry peer review process and has been accepted for publication.

Accepted Manuscripts are published online shortly after acceptance, before technical editing, formatting and proof reading. Using this free service, authors can make their results available to the community, in citable form, before we publish the edited article. This *Accepted Manuscript* will be replaced by the edited, formatted and paginated article as soon as this is available.

You can find more information about *Accepted Manuscripts* in the Information for Authors.

Please note that technical editing may introduce minor changes to the text and/or graphics, which may alter content. The journal's standard Terms & Conditions and the Ethical guidelines still apply. In no event shall the Royal Society of Chemistry be held responsible for any errors or omissions in this *Accepted Manuscript* or any consequences arising from the use of any information it contains.

ROYAL SOCIETY OF CHEMISTRY

www.rsc.org/advances

Cite this: DOI: 10.1039/c0xx00000x

www.rsc.org/xxxxxx

ARTICLE TYPE

Influence of Electronic *vs.* Steric Factors on the Solid-State Photochromic Performances of New Polyoxometalate/Spirooxazine and Spiropyran Hybrid Materials

Clotilde Menet,[a] Hélène Serier-Brault,[a] Olivier Oms,[b] Anne Dolbecq,[b] Jérôme Marrot,[b] Ali Saad,[b] Pierre Mialane,*[b] Stéphane Jobic,[a] Philippe Deniard[a] and Rémi Dessapt*[a]

Received (in XXX, XXX) Xth XXXXXXXXX 20XX, Accepted Xth XXXXXXXXX 20XX
DOI: 10.1039/b000000x

Two new photochromic hybrid organic-inorganic supramolecular materials $(SN)_2[W_6O_{19}]$ (**SN_2W_6**) and $(SP)_2[W_6O_{19}]\cdot 0.5CH_3CN$ (**SP_2W_6**) have been elaborated by combining for the very first time an isopolyoxotungstate $[W_6O_{19}]^{2-}$ with both photoswitchable cationic spirooxazine (SN) and spiropyran (SP), via electrostatic interactions. $(SN)_2[Mo_6O_{19}]$ (**SN_2Mo_6**), a third new photochromic compound which contains the $[Mo_6O_{19}]^{2-}$ unit, has been also designed. Their structure was solved by single-crystal X-ray diffraction analysis, and their solid-state photochromic properties in ambient conditions were thoroughly investigated by UV-visible diffuse reflectance spectroscopy. **SN_2W_6** and **SN_2Mo_6** have been proved to be isostructural while **SP_2W_6** is isostructural with its already reported counterpart **SP_2Mo_6**. In the SN_2M_6 and SP_2M_6 series, the SN and SP molecules are in very close contact with the POM units, which *a priori* should dramatically limit their photoisomerization in the solid state. However, this latter strongly varies with the nature of the metal in the $[M_6O_{19}]^{2-}$ unit. Indeed **SN_2W_6** and **SP_2W_6** exhibit remarkable photochromism under low-power UV excitation (λ_{ex} = 365 nm) while **SN_2Mo_6** and **SP_2Mo_6** develop very limited color-change effects under similar UV exposure. These results have unambiguously highlighted that the efficiency of the SN and SP photoisomerizations in these hybrid systems is much more impacted by an electronic factor resulting from the intrinsic optical absorption properties of both SP and POM components than by a steric factor induced by crystal packings.

1. INTRODUCTION

In recent years, considerable efforts have been made to elaborate efficient solid-state photochromic materials that exhibit reversible light-induced switch between two optically distinguishable states.[1] The ability to control their optical properties with light is of great interest in a wide range of technological and marketable applications, such as smart pigments for paints and windows,[2] optical switches,[3] and more recently, 3D high-density optical data storage.[4] For all these listed applications, ideal materials should develop an efficient photoactivity in the solid state and in ambient conditions (strong coloration contrast, optical bistability, fast photoswitch rates, high cyclability). Currently several organic molecules possess attractive photoswitchable properties but many do not meet all the criteria. For example, the classes of spiropyrans[5] (SP) and spirooxazines[6] (SN) have probably been the most widely studied in these last fifty years, because of their high optical performances and their synthetic accessibility. Such molecules absorb UV irradiation in the 350-400 nm range, and exhibit efficient ring-opening/ring-closure processes between a nonplanar colorless closed form and a coloured opened merocyanin (MC) form (Fig. 1a). MC exhibits a broad absorptic band in the visible domain and can be converted back into the closed-ring form by visible-light irradiation or heating. These reversible photoisomerizations are generally highly efficient i solution or in crystalline state but only at very low temperature. Actually, in most cases, SP and SN solid-state photochromism is weak or totally annihilated in ambient conditions, which strongly

RSC Advances Accepted Manuscript

limits the incorporation of such molecules into efficient photoadressable solid devices. Last decades, several innovative strategies were successfully managed to increase the photochromic activities of spiro-derivative molecules in the solid state. For example, the embedding of spiropyrans and spirooxazines into the cavities of porous organic polymers or sol-gel host matrixes leads to amorphous soft materials with strong photoresponses.[8] The elaboration of crystallized hybrid systems is an alternative approach which, besides, allows the X-ray structural determination of the spiro-derivative/host matrix interface, opening the way to the establishment of fine structure/property relationships.

Recently, we evidenced that the coupling with polyoxometalates (POMs) constitutes an attractive opportunity to reach such crystallized hybrid materials, and to drastically improve the solid-state photochromic performances of spiro-derivatives at room temperature. POMs are described as soluble metal-oxides of early transition metals (usually W, Mo, V) in high oxidation states.[9] The huge diversity of their compositions, structures, charges and sizes make them relevant for applications in numerous fields in optic, which include photochromism,[10] electrochromism,[11] NLO,[12] and photoluminescence.[13] Focusing on photochromism, it has been shown that the assembly of POMs with SP molecules can in some cases exalt the SP → MC photoconversion because of the strong stabilization of the zwitterionic MC form in polar POM frameworks. Noticeably, innovative bistable materials with remarkable photoresponses were obtained from spiropyrans and spirooxazines initially nonphotochromic in their crystalline state.[14] Two new classes of hybrid materials were conceived from two complementary synthesis strategies. The *covalent* approach consisted in grafting via peptidic bonds one or two neutral SP molecules onto an Anderson-type $\{MnMo_6O_{18}\}$ platform.[15] The first multi-photochromic single molecule incorporating one SP and one SN fragments onto a POM core has been even successfully obtained.[16] In a second *ionic* approach, supramolecular SP/POM assemblies were designed by associating a cationic spiropyran (SP) with different polyoxomolybdates via electrostatic interactions.[17] Strikingly, the SP ⇆ MC photoconversion efficiency strongly varies in such ionic hybrid systems. For example, $(SP)_4[Mo_8O_{26}]\cdot 2CH_3CN$ and $(SP)_3(NH_4)[Mo_8O_{26}]$ are remarkably photochromic, while $(SP)_2[Mo_6O_{19}]\cdot 0.5CH_3CN$ (**SP_2Mo_6**) exhibits a very limited UV-induced color-change effect.[17a]

Overall, the photochromic performances of the SP/POM assemblies are governed by both steric and electronic factors. The first one reflects the relative arrangement of the SP cations and the POM units in the frameworks, while the second one refers to the relative positioning of their absorption bands in wavelength space. For example, the weak photochromic performances of **SP_2Mo_6** were assumed to result from a negative combination of these two factors. In contrast with best photochromic systems, the SP cations and the $[Mo_6O_{19}]^{2-}$ units are strongly linked via π-π stacking interactions. This specific arrangement dramatically limits the free volume around the SP molecules and should disadvantage their photoisomerization. In addition, the absorption bands of the $[Mo_6O_{19}]^{2-}$ anion strongly overlap those of the SP cation in the UV domain. Consequently, $[Mo_6O_{19}]^{2-}$ should dramatically absorb the UV excitation energy needed to activate the ring-opening process of the spiropyran.

To date, the influence of both electronic and steric factors on the photochromism efficiency of the SP/POM assemblies have not been uncorrelated because both factors vary in all reported materials. Herein, the main goal of the present work is to specifically investigate the effect of the electronic factor, everything else being equal. For a given topology, the absorption bands of the POMs vary in energy with the nature of the metal.[18] Then, the substitution of Mo by W in the POM units appears as a very useful tool to tune the electronic factor without any structural change. Furthermore, the combination of spiropyrans and spirooxazines with isopolyoxotungstates using the *ionic* approach has never been explored so far. With this aim, we report the synthesis of a new supramolecular system $(SP)_2[W_6O_{19}]\cdot 0.5CH_3CN$ (**SP_2W_6**) which is built upon the same SP cation (Fig. 1a) associated with the $[W_6O_{19}]^{2-}$ unit. Noticeably, **SP_2W_6** is isostructural with **SP_2Mo_6**, what allows keeping constant the steric factor.

To extend our study to other spiro-derivatives, we have also designed two new isostructural hybrid systems $(SN)_2[W_6O_{19}]$ (**SN_2W_6**) and $(SN)_2[Mo_6O_{19}]$ (**SN_2Mo_6**) which combine for the very first time POMs units and a rare cationic spirooxazine (SN) derivative (Fig. 1a). The high photochromic performances of spirooxazines are well-recognized and have found applications in ophthalmology, being used for example in Orgavert™ sunglasses and in PHOTOLITE™ photochromic lenses.[5a] It has also been noticed that while the structure of SN and SP are close, their photochromic properties can differ both on a photogenerated hue and a coloration rate point of view.[16] The structural characterizations of **SP_2W_6**, **SN_2W_6**, and **SN_2Mo_6** are thus reported. Besides, their optical properties are widely discussed and compared with those of **SP_2Mo_6**. This study reveals that, in strong contrast with their Mo counterparts, **SN_2W_6** and **SP_2W_6** exhibit remarkable solid-state photochromism in ambient conditions.

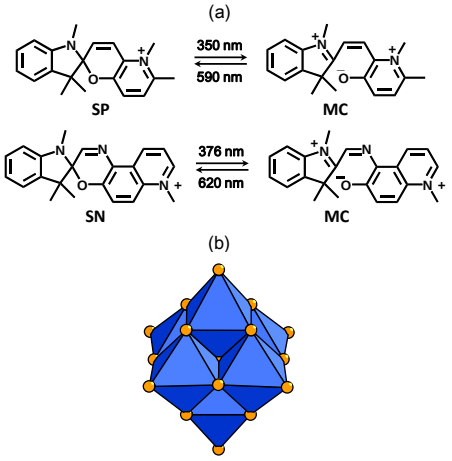

Fig. 1. (a) Photoinduced equilibriums involving the cationic spiropyran (SP) and spirooxazine (SN). (b) Polyhedral representation of the $[M_6O_{19}]^{2-}$ (M = Mo, W) Linqvist-type polyoxometalate (gold sphere: oxygen).

This journal is © The Royal Society of Chemistry [year]

RSC Advances Accepted Manuscript

2. RESULTS AND DISCUSSION

2.1. Synthesis and structural description

$(SP)_2[W_6O_{19}]\cdot 0.5CH_3CN$ (**SP_2W_6**), $(SN)_2[W_6O_{19}]$ (**SN_2W_6**), and $(SN)_2[Mo_6O_{19}]$ (**SN_2Mo_6**) all contain the Lindqvist-type $[M_6O_{19}]^{2-}$ anion[19] (M = Mo or W) (Fig. 1b) which is built upon six edge-shared $[MO_6]$ octahedra. Yellow-ochre powder of **SP_2W_6** has been isolated from a method derived on the synthesis of $(SP)_2[Mo_6O_{19}]\cdot 0.5CH_3CN$ (**SP_2Mo_6**),[17a] starting from $(NBu_4)_2[W_6O_{19}]$ and two equivalents of $SP(NO_3)$ dissolved in acetonitrile. Orange single crystals have been also obtained using slow diffusion of ethanol into the filtrate. **SN_2W_6** and **SN_2Mo_6** have been synthesised starting from $(NBu_4)_2[M_6O_{19}]$ and two equivalents of $SN(NO_3)$ dissolved in DMF. Orange-red single crystals of **SN_2W_6** and red single crystals of **SN_2Mo_6** have been directly obtained from the solutions using slow diffusion crystallization techniques. Elemental analyses, TGA/DSC measurements (Fig. S1, ESI†), and IR spectroscopy analyses (Fig. S2, ESI†) show that these two latter compounds are free from crystallized DMF molecules. Importantly, the coupling of the SP and SN molecules with the $[M_6O_{19}]^{2-}$ anion has a beneficial effect on the thermal resistance of the photoswitchable organic molecules. **SN_2W_6** and **SN_2Mo_6** decompose at 245°C and 250°C respectively, whereas $SN(NO_3)$ is thermally stable up to 190°C only. Similarly, **SP_2W_6** and **SP_2Mo_6** decompose at 240°C and 255°C respectively, while $SP(NO_3)$ is thermally stable up to 200°C only.

Crystal structures of SP_2W_6, SN_2Mo_6, and SN_2W_6. Single-crystal X-ray diffraction analysis of **SP_2W_6** reveals that this new compound is isostructural with **SP_2Mo_6**. **SP_2W_6** is built upon isolated $[W_6O_{19}]^{2-}$ units, SP cations and crystallized acetonitrile molecules that are assembled in a supramolecular framework. The $[W_6O_{19}]^{2-}$ entities are well surrounded by the SP cations which interact with the POM surfaces via electrostatic interactions and C–H···O contacts (Fig. 2a). In particular, the planar methylpyridinium rings of two SP ions and the oxygen facets of the $[W_6O_{19}]^{2-}$ unit perfectly face each other with a very low dihedral angle (α = 4.0°), and the shortest C···O distance of 3.389(3) Å. These values are quite comparable with those observed for **SP_2Mo_6** ($d_{C\cdots O}$ = 3.372(5) Å, and α = 4.4°).

The isostructural compounds **SN_2W_6** and **SN_2Mo_6** are built upon $[M_6O_{19}]^{2-}$ blocks and SN cations (Fig. 2b). The structure of **SN_2W_6** has been arbitrary chosen to describe the crystal packing of this series. The $[W_6O_{19}]^{2-}$ anions are well separated from each other in a cage-like supramolecular organic framework delimited by the SN cations (the shortest O···O distance between two adjacent $[W_6O_{19}]^{2-}$ units is 5.67 Å). The methylpyridinium group of four SN cations are quite parallel with the oxygen facets of the $[W_6O_{19}]^{2-}$ block and they interact together in a large contact zone, with a short interplanar distance (shortest C···O distance of 2.970(5) Å), and a low dihedral angle (α = 7.5°). These values match very well with those observed for **SN_2Mo_6** ($d_{C\cdots O}$ = 2.954(1) Å, and α = 7.0°).

To sum up, the structural studies of the SP_2M_6 and SN_2M_6 series well evidence that the spiro-molecules undergo very strong geometrical constraints, due to their very close proximity with the $[M_6O_{19}]^{2-}$ units, which should *a priori* be highly unfavourable for efficient photoisomerization. Nevertheless in each series, the organic cations interact with the POMs in a comparable way, enabling to maintain constant the steric factor, and to specifically investigate the influence of the nature of the metal in the POM unit, and thus the electronic factor, on the solid-state photochromic performances.

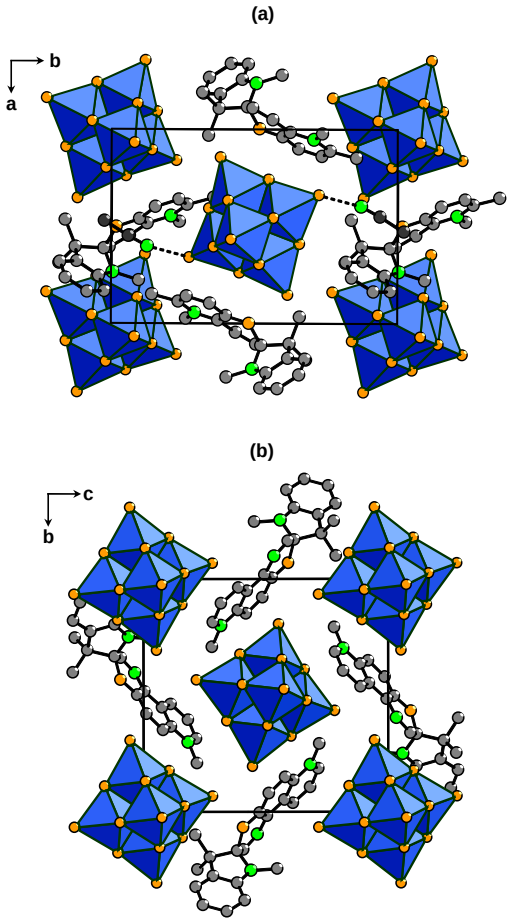

Fig. 2. Mixed polyhedral and ball-and-stick representations of the crystal packing in (a) **SP_2W_6** and (b) **SN_2W_6** showing the interactions between the π-donor methylpyridinium groups of the SP and SN cations and the $[W_6O_{19}]^{2-}$ oxygen facets. (blue octahedra = WO_6, grey spheres: carbons of SP and SN cations; dark spheres: carbons of acetonitrile molecules; green sphere: nitrogen; gold sphere: oxygen). N···O interactions between acetonitrile molecules and $[W_6O_{19}]^{2-}$ units in **SP_2W_6** are displayed as dotted lines. The hydrogen atoms are omitted for clarity.

2.2 Optical properties

Optical properties before UV irradiation. The optical properties of **SP_2W_6**, **SP_2Mo_6**, **SN_2W_6** and **SN_2Mo_6** before UV irradiation have been investigated in ambient conditions by diffuse reflectance spectroscopy of microcrystalline powders. The main optical characteristics of the four hybrid systems are gathered in Table 1. Fig. 3 displays the absorption spectra of **SP_2W_6** and **SP_2Mo_6** compared with those of the iodide salt of the SP cation SP(I) and the $(NBu_4)_2[M_6O_{19}]$ salts that contain similar $[M_6O_{19}]^{2-}$ units without SP entities. As previously discussed,[17] the absorption spectrum of **SP_2Mo_6** (Fig. 3a) in the UV domain is the sum of the absorption bands of the SP cation (for which the

RSC Advances Accepted Manuscript

low-energy absorption is located at $\lambda_{max}^{(spiro)}$ = 350 nm), and the broad ligand-to-metal charge-transfer (LMCT) transitions of the $[Mo_6O_{19}]^{2-}$ anion[18] ($\lambda^{(POM)}$ = 269 and 327 nm). The absorptions of both POM and SP moieties exhibit a significant degree of overlapping which can be well assessed by introducing the $\Delta\lambda$ parameter defined as $\Delta\lambda = \lambda_{max}^{(spiro)} - \lambda_{max}^{(POM)}$, with $\lambda_{max}^{(POM)}$ the low-energy LMCT transition centred on the POM unit. **SP_2Mo_6** is then characterized by a very small $\Delta\lambda$ value (23 nm). In strong contrast, for **SP_2W_6** (Fig. 3b), the LMCT transitions of $[W_6O_{19}]^{2-}$ are located at much higher energies than those of $[Mo_6O_{19}]^{2-}$ i.e., $\lambda^{(POM)}$ = 220 nm (not shown in Fig. 3b) and 280 nm,[18] and then, the $\Delta\lambda$ value significantly increases to reach 70 nm. Furthermore, the $[W_6O_{19}]^{2-}$ anion does not absorb at $\lambda_{max}^{(spiro)}$ = 350 nm. A similar effect is observed in the SN_2M_6 series (Figure S3, ESI†). Indeed, $\Delta\lambda$ = 48 and 95 nm for **SN_2Mo_6** and **SN_2W_6**, respectively. These values are higher than those of **SP_2Mo_6** and **SP_2W_6** because SN absorbs at a higher wavelength ($\lambda_{max}^{(spiro)}$ = 375 nm) than SP. In summary, the electronic factor is strongly modified by substituting Mo by W in the SP_2M_6 and SN_2M_6 series. This leads to a better separation in energy between the absorption bands of both organic and inorganic components in the UV domain. Consequently, in marked contrast with its Mo counterpart, the $[W_6O_{19}]^{2-}$ anion does not compete with SP and SN to absorb the excitation UV energy at λ_{ex} = 365 nm needed to activate their ring-opening processes.

Table 1. Characteristic optical parameters of the SP_2M_6 and SN_2M_6 series.

	SP_2Mo_6	**SP_2W_6**	**SN_2Mo_6**	**SN_2W_6**
$\lambda_{max}^{(POM)}$ (nm)[a]	327	280	327	280
$\lambda_{max}^{(spiro)}$ (nm)	350	350	375	375
$\Delta\lambda$ (nm)[b]	23	70	48	95
λ_{CT} (nm)[c]	430-540	400-510	430-590	420-560
color[d]	brown-ochre	yellow-ochre	red-ochre	brown-ochre

[a]Lower energy POM LCMT transition. [b]$\Delta\lambda = \lambda_{max}^{(spiro)} - \lambda_{max}^{(POM)}$. [c]Range of wavelength for the Charge-Transfer transition. [d]Color of powdered sample before UV irradiation.

The absorption spectra of **SP_2W_6**, **SN_2W_6** and **SN_2Mo_6** also exhibit an additional weak absorption band in the range 400-600 nm (Table 1), which is responsible for the color of powdered materials. This absorption is ascribed to an intermolecular Charge-Transfer (CT) transition between the electron-rich "π-donor" spiro-derivative and the electron-poor $[M_6O_{19}]^{2-}$ "acceptor", due to their close proximity in the solid-state (see above).[17a] The CT band totally disappears when the samples are dissolved in highly polar solvents such as DMSO, and the resulting spectra exactly match the sum of the absorption spectra of isolated organic and $[M_6O_{19}]^{2-}$ ions (Fig. S4, ESI†). For a given electron-donor organic molecule, the energy of the CT transition increases with that of the LMCT band of the associated POM unit.[17a] Then, λ_{CT} are systematically blue-shifted in **SN_2W_6** and **SP_2W_6**, and the color of these two powdered samples are less pronounced than those of their Mo counterparts (Fig. S5, ESI†), enabling us to speculate a better coloration contrast during the photochromic process.

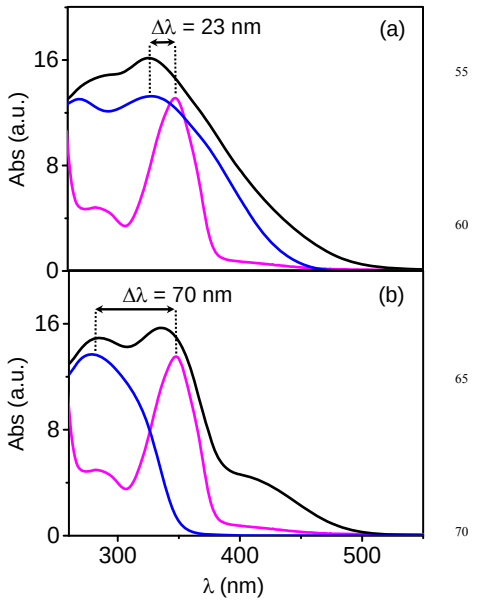

Fig. 3. Normalized Kubelka-Munk transformed reflectivity spectra before UV irradiation of (a) **SP_2Mo_6** (black), SP(I) (magenta), and $(TBA)_2[Mo_6O_{19}]$ (blue), and (b) **SP_2W_6** (black), SP(I) (magenta), and $(TBA)_2[W_6O_{19}]$ (blue). The $\Delta\lambda$ parameter is defined as $\Delta\lambda = \lambda_{max}^{(spiro)} - \lambda_{max}^{(POM)}$, with $\lambda_{max}^{(POM)}$ the low-energy LMCT transition of the POM unit.

Solid-state photochromic properties. First, the photochromic properties of **SP_2W_6** and **SP_2Mo_6** in ambient conditions have been compared (Fig. 4). While the color-change effect of **SP_2Mo_6** is very limited under low-power near UV excitation (λ_{ex} = 365 nm),[17a] **SP_2W_6** exhibits a remarkably improved photochromic response under similar UV exposure (Fig. 4a). The color of the yellowish-ochre powder gradually shifts to purple-brown with a high coloration contrast and a fast coloration speed. Similarly as observed for **SP_2Mo_6**, the color change of **SP_2W_6** deals with the appearance of the MC form of the SP cation that is optically characterized by an absorption band arising at $\lambda_{max}^{(MC)}$ = 590 nm (Fig. 4b). This quite evidences that, even if both materials are isostructural, the SP → MC photoisomerization is much more efficient in **SP_2W_6** than in **SP_2Mo_6**. This can be explained considering that in the case of **SP_2Mo_6**, most of the incident UV-light flow is strongly absorbed by the POM unit, and the resulting incident UV-light flow, available for the SP → MC photoisomerization, is much more limited than for **SP_2W_6**. Thus, the concentration of the photogenerated MC form is weaker in the hybrid polyoxomolybdate, and consequently, its color-change effect is dramatically affected. Furthermore, let us also noticed that the $[M_6O_{19}]^{2-}$ units do not contribute to the photogenerated coloration because, in contrast with the known photochromic polyoxometalate/organoammonium hybrid materials,[10] their photoreduction does not occur in SP/POM assemblies.

The solid-state photochromic properties of **SN_2W_6**, and **SN_2Mo_6** in ambient conditions exactly follow the same trend (Fig. 5). Noticeably, the brown-ochre powder of **SN_2W_6** gradually changes to dark-green under UV excitation at λ_{ex} = 365 nm (Fig. 5a). The photochromic effect that is detectable with

RSC Advances Accepted Manuscript

This journal is © The Royal Society of Chemistry [year]

naked eyes after only 2 s, finally reaches a saturation level after only 10 min, revealing a very fast photoresponse and a remarkable coloration contrast, even more pronounced than those of **SP_2W_6**. The intense photogenerated absorption band of the MC form of the SN cation is located at $\lambda_{max}^{(MC)}$ = 620 nm in **SN_2W_6** (Fig. 5b). This band is also observable in the optical spectrum of **SN_2Mo_6** (Fig. S6, ESI†) but its intensity is much weaker. This latter compound develops very limited photochromic performances, and the color-change effect remains hardly detectable by naked eyes.

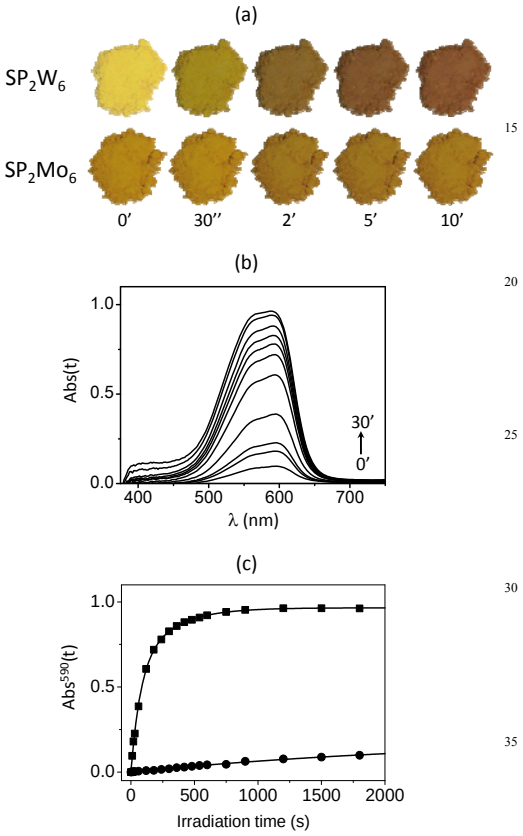

Fig. 4. (a) Photographs of powders of **SP_2W_6**, and **SP_2Mo_6** at different time (in min) during the coloration process under UV light (λ_{ex} = 365 nm). (b) Temporal evolution of the absorption at 590 nm for **SP_2W_6** after 0, 0.166, 0.333, 0.5, 1, 2, 3, 4, 5, 7, 10, and 30 min of 365 nm-UV irradiation. (c) Experimental (point) and fitted (line) $Abs^{590}(t)$ vs. *t* plots for **SP_2W_6** (■), and **SP_2Mo_6** (●).

The coloration kinetics of the four hybrid systems have been quantified at room temperature by monitoring the photogenerated absorption at $\lambda_{max}^{(MC)}$ ($Abs^{\lambda max}(t)$) as a function of the UV irradiation time *t*. The $Abs^{\lambda max}(t)$ *vs t* plots have been adequately fitted using a biexponential rate law[16, 17a] (Fig. 4c and Fig. 5c for the SP_2M_6 and SN_2M_6 series, respectively), and the kinetics parameters are gathered in Table S1, ESI†. The photocoloration rates of the compounds can be well compared by considering their half-life time ($t_{1/2}$) namely the UV irradiation time required for $Abs^{\lambda max}(t)$ to reach half of its maximum value. **SN_2W_6** exhibits the most effective photocoloration process, much more intense and faster than the three other compounds. Importantly, its photocoloration rates ($t_{1/2}$ = 0.8 min) is twenty times faster than that of **SN_2Mo_6** ($t_{1/2}$ = 16.0 min). In the SP_2M_6 series, the photocoloration rate is about eleven more times faster for **SP_2W_6** ($t_{1/2}$ = 1.3 min) than for **SP_2Mo_6** ($t_{1/2}$ = 15.0 min). This quite evidences that the SP and SN photoisomerization rates are drastically improved by substituting $[Mo_6O_{19}]^{2-}$ by $[W_6O_{19}]^{2-}$ in both series, despite the strong steric constraints applied to the spiro-derivative molecules by the POM framework.

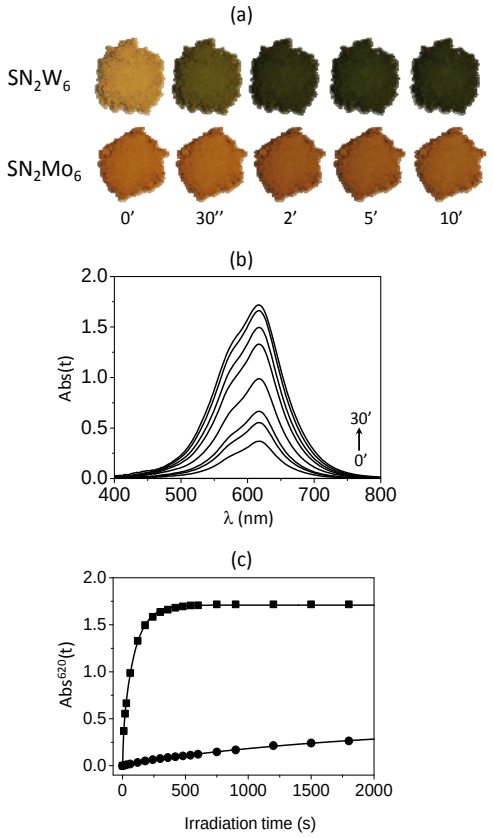

Fig. 5. (a) Photographs of powders of **SN_2W_6**, and **SN_2Mo_6** at differe time (in min) during the coloration process under UV light (λ_{ex} = 365 nm). (b) Temporal evolution of the absorption at 620 nm for **SN_2W_6** after 0, 0.166, 0.333, 0.5, 1, 2, 3, 6, and 10 min of 365 nm-UV irradiation. (c) Experimental (point) and fitted (line) $Abs^{620}(t)$ vs. *t* plots for **SN_2W_6** (■), and **SN_2Mo_6** (●).

The fading kinetics of **SN_2W_6** and **SP_2W_6** have been also investigated at room temperature to evaluate the efficiency of the MC → SN and MC → SP back conversions in the dark (thermal fading), and under visible-light irradiation at 630 and 590 nm, respectively, i.e. with energies corresponding to the absorption band of the MC forms of the SN and SP ions. The $Abs^{\lambda max}(t)$ *vs t* plots of the coloration and fading processes are displayed in Fig. 6a for **SN_2W_6** and Fig. S7, ESI† for **SP_2W_6**. Decays have bee well fitted using a biexponential rate law, (see Table S2, ESI† for the detailed fading kinetic parameters). The fading rates have been compared by considering their fading half-life time. Und visible-light irradiation, **SN_2W_6** and **SP_2W_6** exhibit very fast and full bleaching processes. Very interestingly, the fading rates are comparable with the coloration ones (for the bleaching proces $t_{1/2}$ = 0.6 and 0.2 min for **SN_2W_6** and **SP_2W_6**, respectively). I strong contrast, both hybrid systems develop very limited therma

RSC Advances Accepted Manuscript

fading processes. Indeed, the maximum of absorption loss after 2 hours reaches only 6% for $\mathbf{SN_2W_6}$ and 8% in the case of $\mathbf{SP_2W_6}$, revealing that after switching off the UV irradiation, most of the MC forms remain stabilized in the polar hybrid POM framework. Hence, $\mathbf{SN_2W_6}$ and $\mathbf{SP_2W_6}$ are quasi-bistable at room temperature.

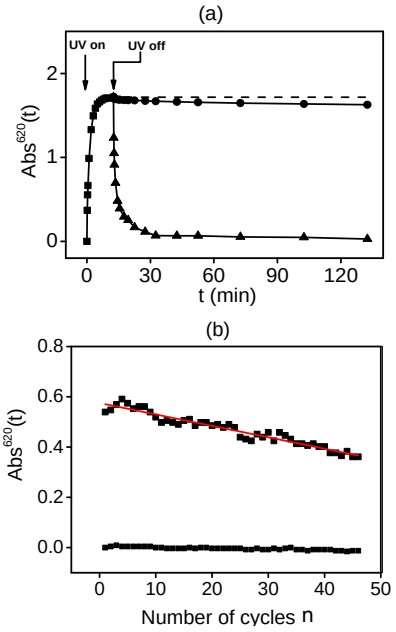

Fig. 6. (a) Comparison of the temporal evolutions of the absorbance at 620 nm for $\mathbf{SN_2W_6}$ under red light (λ_{ex} = 630 nm) (▲) and in the dark (●) for a sample initially irradiated for 10 min with UV light (λ_{ex} = 365 nm) (■). The dashed line shows the absorbance value just before switching off the UV light. (b) Evolution of the absorbance monitored at 620 nm for $\mathbf{SN_2W_6}$ during successive coloration/bleach cycles at room temperature. In each cycle, the sample was irradiated for 1 min with UV light (λ_{ex} = 365 nm), and then for 10 min with red light (λ_{ex} = 630 nm). The red line corresponds to the linear fit of $Abs^{620}(n)$ *vs* n (R^2 = 0.965).

Finally, the robustness of $\mathbf{SN_2W_6}$ and $\mathbf{SP_2W_6}$ for repeatable "recording-erasing" processes at room temperature was investigated by monitoring the evolution of $Abs^{\lambda max}$ of samples alternatively irradiated under UV light and visible light. We managed to perform a long study of cyclability by following the variation of the absorption on approximately fifty cycles, what to our knowledge, was never reported for powdered photochromic samples so far. In the case of $\mathbf{SN_2W_6}$, the evolution of $Abs^{620}(n)$ *vs* n, *i.e.*, the number of coloration/fading cycles, reveals that this hybrid system shows a good cyclability with a high coloration contrast (Fig. 6b). For each cycle, the bleaching process is full, but a fatigue is observed during the successive photocoloration processes. The photogenerated absorption progressively decreases with n, and the absorption loss is about 33% at the end of fifty cycles. Surprisingly, the decrease of $Abs^{620}(n)$ with n, can be fitted with the empirical linear relationship described in equation (1). This relationship allows predicting that the variation of absorption between both colorless and colored states should be zero at the end of 128 cycles.

$$Abs^{620}(n) = -0.0045n + 0.5751 \quad (1)$$

The photocoloration fatigue is more marked for $\mathbf{SP_2W_6}$, and the absorption loss reaches about 50% at the end of fifty cycles (Fig. S7b, ESI†). Similarly, $Abs^{590}(n)$ linearly decreases with n according to equation 2, revealing that the color-change effect should disappear at the end of 98 cycles.

$$Abs^{590}(n) = -0.0040n + 0.3916 \quad (2)$$

At first sight, the poorer cyclability of $\mathbf{SP_2W_6}$ could result from the presence of the crystallized acetonitrile molecules which is expected to introduce some flexibility in the hybrid framework.

3. CONCLUSION

In conclusion, the two first supramolecular hybrid isopolyoxotungstates $\mathbf{SN_2W_6}$ and $\mathbf{SP_2W_6}$ have been successfully designed by assembling the Linqvist-type $[W_6O_{19}]^{2-}$ unit with cationic spirooxazine and spiropyran. Noticeably, while the SN and SP ions undergo strong steric constraints in the frameworks, these systems exhibit remarkable solid-state photochromic properties in ambient conditions, which include high photocoloration contrasts, fast coloration and fading rates, and good cyclabilities. Besides, $\mathbf{SN_2W_6}$ and $\mathbf{SP_2W_6}$ are quasi-bistable systems at room temperature, and they possess high light-driven "recording-erasing" potentialities. Strikingly, their photochromic performances are drastically improved compared to $\mathbf{SN_2Mo_6}$ and $\mathbf{SP_2Mo_6}$, their isostructural Mo counterparts, revealing that the photoisomerization of the spiro-molecules is much more impacted by the electronic factor than by the steric one. In strong contrast with $[Mo_6O_{19}]^{2-}$, the high-energy LMCT transition of $[W_6O_{19}]^{2-}$ does not overlap the absorption of the SN and SP cations in the UV domain, and both organic and inorganic components do not compete to absorb the excitation UV light.

The findings may open a new pathway for the design of supramolecular SP or SN/POMs assemblies with outstanding solid-state photochromic properties. Importantly, they quite evidence that efficient photochromic hybrid systems can be designed even if their crystal packings are *a priori* highly unfavourable for the photoisomerization of the spiro-molecules. In addition, the substitution of Mo by W is a very useful tool to favourably tune the electronic factor. We are currently working to characterize the structure of $\mathbf{SP_2W_6}$ and $\mathbf{SN_2W_6}$ in their colored forms using single-crystal X-ray photodiffraction analyses. Exploitation of the remarkable photochromic properties of $\mathbf{SN_2W_6}$ and $\mathbf{SP_2W_6}$ is also now under investigation. In particular, their integration into organic polymers or as thin film to elaborate photonic devices and sensors will be considered. This kind of immobilisation is also expected to increase the resistance to "fatigue".[20] In addition, the synthesis of new supramolecular assemblies built upon other isopolyoxotungstates varying in shape, size and charge are currently under study. Finally, new hybrid systems, based on polyoxotungstates and photoactive organic dyes associating both photochromism and fluorescence are also underway.

4. EXPERIMENTAL SECTION

Synthesis. $SP(NO_3)$,[21] SN(I),[22] $(NBu_4)_2[W_6O_{19}]$[23] and $(NBu_4)_2[Mo_6O_{19}]$[24] have been synthesized according to the

This journal is © The Royal Society of Chemistry [year]

RSC Advances Accepted Manuscript

reported procedures.

$SN(NO_3)$. SN(I) (1 g, 2.1 mmol) was dissolved in a cosolvent $MeOH/CH_3CN$ (30/25 mL) (solution 1). $AgNO_3$ (360 mg, 2.1 mmol) was dissolved in MeOH (15 mL) (solution 2). Solution 2 was added dropwise to solution 1 under stirring leading to the precipitation of a yellow solid of AgI. The solution was filtered through a short plug of celite to afford an oily solution after removal of the solvent under reduced pressure. The solution was then precipitated in ether and the brown powder obtained was washed with ether and dried in air. $SN(NO_3)$ was obtained in 40% yield. ^{1}H NMR (300 MHz, $CDCl_3$) δ (ppm) 9.82 (d, 1H), 9.60 (d, 1H), 8.30 (d, 1H), 8.1 (dd, 1H), 7.92 (s, 1H), 7.7 (d, 1H), 7.11 (d, 1H), 6.97 (t, 1H), 6.62 (d, 1H), 4.84 (s, 1H), 2.77 (s, 3H), 1.40 (s, 3H), 1.36 (s, 3H).

$(SN)_2[Mo_6O_{19}]$ (**SN_2Mo_6**). $(NBu_4)_2[Mo_6O_{19}]$ (220 mg, 0.16 mmol) was dissolved in DMF (9 mL). The solution (solution 1) was stirred for a few minutes at room temperature. In addition, a second solution (solution 2) was obtained by dissolving $SN(NO_3)$ (150 mg, 0.37 mmol) in DMF (5 mL) at room temperature. Solution 2 was added dropwise to solution 1 under vigorous stirring. The mixture was stirred at 40°C for two hours, kept at room temperature, and then filtered. Crystallization of the product by diffusion of ethanol into the filtrate gave suitable single crystals for X-Ray diffraction. Yield in Mo: 64 %. *Anal*. Calcd for $C_{44}H_{44}O_{21}N_6Mo_6$: C, 33.42 ; H, 2.78 ; N, 5.32. Found: C, 33.38 ; H, 2.80 ; N, 5.29. FT-IR (KBr, cm^{-1}): SN cations 1629 (m), 1604 (s), 1584 (s), 1531 (m), 1487 (s), 1467 (m), 1441 (m), 1425 (m), 1394 (s), 1368 (m), 1349 (sh), 1306 (m), 1284 (s), 1237 (m), 1189 (w), 1169 (m), 1147 (m), 1130 (m), 1119 (w), 1108 (sh), 1079 (m), 1055 (s), 1023 (m), 1003 (w) ; υMo=O, υMo-O-Mo 959 (vs), 928 (sh), 912 (w), 892 (w), 796 (vs), 751 (s), 682 (w), 655 (w), 623 (sh), 600 (m), 577 (m), 538 (m), 522 (sh), 477 (sh), 463 (m), 437 (m). From ATG/DSC measurements, **SN_2Mo_6** is stable up to 280°C.

$(SN)_2[W_6O_{19}]$ (**SN_2W_6**). $(NBu_4)_2[W_6O_{19}]$ (305 mg, 0.16 mmol) was dissolved in DMF (8 mL). The solution (solution 1) was stirred for a few minutes at room temperature. In addition, a second solution (solution 2) was obtained by dissolving $SN(NO_3)$ (200 mg, 0.49 mmol) in DMF (5 mL) at room temperature. Solution 2 was added dropwise to solution 1 under vigorous stirring. The mixture was stirred at 40°C for one hour and a half, kept at room temperature, and then filtered. Crystallization of the product by diffusion of ethanol into the filtrate gave suitable single crystals for X-Ray diffraction. Yield in W: 46%. *Anal*. Calcd for $C_{44}H_{44}O_{21}N_6W_6$: C, 25.19 ; H, 2.10 ; N, 4.01. Found: C, 25.15 ; H, 2.07 ; N, 4.06. FT-IR (KBr, cm^{-1}): SN cations 1628 (w), 1601 (m), 1583 (m), 1529 (m), 1487 (s), 1466 (m), 1440 (m), 1424 (m), 1395 (m), 1366 (m), 1347 (sh), 1324 (w), 1305 (m), 1283 (s), 1260 (sh), 1236 (m), 1188 (w), 1168 (m), 1144 (w), 1128 (m), 1119 (w), 1106 (w), 1077 (m), 1056 (m), 1024 (m); υW=O, υW-O-W 980 (vs), 927 (m), 907 (w), 890 (w), 810 (vs), 752 (s), 679 (m), 670 (m), 653 (sh), 632 (sh), 623 (sh), 583 (m), 537 (m), 520 (w), 443 (s). From ATG/DSC measurements, **SN_2W_6** is stable up to 260°C.

$(SP)_2[W_6O_{19}]\cdot 0.5CH_3CN$ (**SP_2W_6**). $(NBu_4)_2[W_6O_{19}]$ (305 mg, 0.16 mmol) was dissolved in acetonitrile (10 mL). The solution (solution 1) was stirred for a few minutes at room temperature. In addition, a second solution (solution 2) was obtained by dissolving $SP(NO_3)$ (200 mg, 0.49 mmol) in acetonitrile (6 mL) at room temperature. Solution 2 was added dropwise to solution 1 under vigorous stirring leading to the slow precipitation of an ochre powder of **SP_2W_6**. The mixture was stirred at 40°C for one hour and a half, kept at room temperature, and then filtered. The powder was washed with acetonitrile and ethanol, and dried in air. Yield in W: 53%. Crystallization of the product by diffusion of ethanol into the filtrate gave suitable single crystals for X-Ray diffraction. *Anal*. Calcd for $C_{41}H_{47.5}O_{21}N_{4.5}W_6$: C, 24.09 ; H, 3.32 ; N, 3.08. Found: C, 24.15 ; H, 3.34 ; N, 3.12. FT-IR (KBr, cm^{-1}): SP cations 1608 (m), 1486 (s), 1472 (m), 1454 (m), 1433 (w), 1386 (w), 1362 (m), 1311 (s), 1297 (s), 1279 (w), 1252 (w), 1236 (w), 1207 (sh), 1190 (w), 1168 (w), 1047 (w), 1017 (w), 1104 (w), 1057 (m), 1025 (m); υW=O, υW-O-W 977 (vs), 926 (m), 915 (m), 878 (w), 810 (vs), 765 (m), 707 (m), 661 (w), 585 (m), 552 (w), 530 (w), 445 (s). From DSC/TGA measurements, **SP_2W_6** loses the acetonitrile molecules above 180°C.

X-ray crystallography: Data collection was carried out by using a Siemens SMART three-circle diffractometer for **SN_2Mo_6** and by using a Bruker Nonius X8 APEX 2 diffractometer for **SN_2W_6** and **SP_2W_6**. Both were equipped with a CCD bi-dimensional detector using the monochromatized wavelength λ(Mo Kα) = 0.71073 Å. Absorption correction was based on multiple and symmetry-equivalent reflections in the data set using the SADABS program[25] based on the method of Blessing.[26] The structures were solved by direct methods and refined by full-matrix least-squares using the SHELX-TL package.[27] Crystallographic data are given in Table 2. CCDC 1414602, 1414603 and 1414604 contain the supplementary crystallographic data for this paper. These data can be obtained free of charge from the Cambridge Crystallographic Data Centre via www.ccdc.cam.ac.uk/data_request/cif.

Table 2. Crystallographic data

	SN_2Mo_6	**SN_2W_6**	**SP_2W_6**
Empirical formula	$C_{44}H_{44}N_6O_{21}Mo_6$	$C_{44}H_{44}N_6O_{21}W_6$	$C_{41}H_{47.5}N_{4.5}O_{21}W_6$
Formula weight [g]	1568.49	2095.95	2042.43
Temperature [K]	298	298	298
Crystal system	Monoclinic	Monoclinic	Monoclinic
Space group	$P2_1/n$	$P2_1/n$	$P2_1/n$
a [Å]	14.3898(6)	14.410(3)	10.4923(2)
b [Å]	12.7305(5)	12.743(3)	15.1018(3)
c [Å]	14.4617(7)	14.549(3)	16.1338(2)
β [°]	111.279(2)	111.339(10)	104.6525(6)
V [Å^3]	2468.6(2)	2488.5(9)	2473.30(7)
Z	2	2	2
ρ_{calc} [g cm^{-3}]	2.110	2.797	2.743
μ [mm^{-1}]	1.566	13.899	13.979
Data / Parameters	7214/353	7253/353	7227/340
R_{int}	0.0353	0.0307	0.0489
GOF	0.959	1.032	1.119
R_1 (>2σ(I))	0.0264	0.0208	0.0320
wR_2	0.0600	0.0563	0.0908

RSC Advances Accepted Manuscript

Physical Measurements. Elemental analyses of the solids were performed by the "Service de microanalyses ICSN CNRS, in Gif sur Yvette (France), and by the "Service d'Analyse du CNRS", in Vernaison (France). FT-IR spectra were recorded in the 4000-400 cm^{-1} range on a BRUKER Vertex equipped with a computer control using the OPUS software. Differential scanning calorimetry (DSC) and thermogravimetric analysis (TGA) were performed by flowing dry argon with a heating and cooling rate of 5°C/min on a SETARAM TG-DSC 111 between 20 and 800°C. Diffuse reflectance spectra were collected at room temperature on a finely ground sample with a Cary 5G spectrometer (Varian) equipped with a 60 mm diameter integrating sphere and computer control using the "Scan" software. Diffuse reflectance was measured from 250 to 1550 nm with a 2 nm step using Halon powder (from Varian) as reference (100% reflectance). The reflectance data were treated by a Kubelka-Munk transformation[28] to obtain the corresponding absorption data. The photocoloration and fading kinetics were quantified by monitoring the temporal evolution of the photogenerated absorption $Abs^{\lambda max}(t)$ defined as $Abs^{\lambda max}(t) = -\log(R^{\lambda max}(t)/R^{\lambda max}(0))$, where $R^{\lambda max}(t)$ and $R^{\lambda max}(0)$ are the reflectances at the time t and at t = 0, respectively. For the coloration kinetics, the samples were irradiated with a Fisher Bioblock labosi UV lamp (λ_{ex} = 365 nm, P = 6W) at a distance of 50 mm. $Abs^{\lambda max}(t)$ *vs. t* plots have been fitted according to a biexponential rate law $Abs^{\lambda max}(t) = (A_1 + A_2) - A_1\exp(-k^c_1 t) - A_2\exp(-k^c_2 t)$, with k^c_1 and k^c_2 the extracted coloration rate constants. For the bleaching processes, the samples were first irradiated under 365 nm-UV excitation for 10 minutes in the case of $\mathbf{SN_2W_6}$, and for 20 minutes in the case of $\mathbf{SP_2W_6}$, times for which the photoinduced absorptions are quasi-saturated. Then, the compounds were put under Thorlabs LED Array light sources (590 nm - 1.4 W/cm^2 and 630 nm - 2.4 W/cm^2) at a distance of 100 mm. The bleaching kinetics were determined at room temperature by monitoring the temporal decays of $Abs^{\lambda max}(t)$ of samples once irradiated $Abs^{\lambda max}(t)$ *vs. t* plots have been fitted according to a biexponential rate law $Abs^{\lambda max}(t) = (A_0 - A_1 - A_2) + A_1\exp(-k^f_1 t) + A_2\exp(-k^f_2 t)$, with k^f_1 and k^f_2 the extracted fading rate constants.

Authors Information

Corresponding Author

[a] *Institut des Matériaux Jean Rouxel, Université de Nantes, CNRS, 2 rue de la Houssinière, BP 32229, 44322 Nantes cedex, France. Fax: +33-240-373-995; E-mail: remi.dessapt@cnrs-imn.fr*

[b] *Institut Lavoisier de Versailles, UMR 8180, Université de Versailles Saint-Quentin en Yvelines, 45 Avenue des Etats-Unis, 78035 Versailles cedex, France. Fax: +33-139-254-381; E-mail: mialane@chimie.uvsq.fr*

† Electronic Supplementary Information (ESI) available: complementary Kubelka-Munk transformed reflectivity and absorption spectra, UV-vis absorption spectra in solution, photocoloration and fading kinetics parameters. See DOI: 10.1039/b000000x/

Acknowledgements. This work was supported by the CNRS, the Ministère de l'Enseignement Supérieur et de la Recherche, the ANR-11-BS07-011-01 BIOOPOM, and the LUMOMAT project supported by the Région des Pays de la Loire.

Notes and references

1 (a) Y. Hirshberg and E. Fisher, *J. Chem. Phys.*, 1955, **23**, 1723. (b) H. Bouas-Laurent, *Photochromism: Molecules and Systems*, Elsevier, Amsterdam, 2003.

2 C. Bechinger, S. Ferrere, A. Zaban, J. Sprague and B. A. Gregg, *Nature,*1996, **383**, 608.

3 B. L. Feringa, *Molecular Switches*; Wiley-VCH: New York, 2001.

4 (a) M. Irie, *Chem. Rev*., 2000, **100**, 1685. (b) S. Kawata and Y. Kawata, *Chem. Rev*., 2000, **100**, 1777. (c) J. A. Delaire and K. Nakatani, *Chem. Rev*., 2000, **100**, 1817. (d) C. C. Corredor, Z.-L. Huang, K. D. Belfield, A. R. Morales and M. V. Bondar, *Chem. Mater*., 2007, **19**, 5165. (e) Y. Yokoyama, *Chem. Rev*., 2000, **100**, 1717.

5 (a) M. Natali and S. Giordani *Chem. Soc. Rev.*, 2012, **41**, 4010. (b) V. I. Minkin, *Chem. Rev*., 2004, **104**, 2751. (c) G. Berkovic, V. Krongauz and V. Weiss, *Chem. Rev*., 2000, **100**, 1741.

6 (a) B. Schaudel, C. Guermeur, C. Sanchez, K. Nakatani and J. A. Delaire, *J. Mater. Chem.*, 1997, **7**, 61. (b) J. Biteau, F. Chaput and J.-P. Boilot, *J. Phys. Chem*., 1996, **100**, 9024. (c) W. Yuan, L. Sun, H. Tang, Y. Wen, G. Jiang, W. Huand, L. Jiang, Y. Song, H. Tian and D. Zhu, *Adv. Mater*., 2005, **17**, 156. (d) R. A. Kopelman, S. M. Snyder and N. L. Franck, *J. Am. Chem. Soc*., 2003, **125**, 13684.

7 J. Harada, Y. Kawazoe and K. Ogawa, *Chem. Commun.*, 2010, **46**, 2593.

8 (a) B. Osterby, R. D. McKelvey and L. Hill *J. Chem. Edu. 1991, **68**, 424.* (b) D. Levy, *Chem. Mater*. 1997, **9**, 2666. (c) C. Sanchez, B. Lebeau, F. Chaput and J.-P. Boilot, *Adv. Mater*. 2003, **15**, 1969. (d) M.-Q. Zhu, L. Zhu, J. J. Han, J. K. Hurst and A. D. Q. Li, *J. Am. Chem. Soc*. 2006, **128**, 4303. (e) I. Khale, O. Tröber, S. Trentsch, H. Richter, B. Grünler, S. Hemeltjen, M. Schlesinger, M. Mehring and S. Spange, *J. Mater Chem*. 2011, **21**, 5083.

9 (a) Polyoxometalate Chemistry: From Topology via Self-Assembly to Applications (Eds M. T. Pope, A. Müller), KLUWER, Dordrecht, Netherlands, 2001. (b) Polyoxometalate Chemistry for Nano-Composite Design, (Eds. T. Yamase, M. T. Pope), KLUWER, New York, 2002. (c) Polyoxometalate Molecular Science, (Eds J. J. Borras-Almenar, E. Coronado, A. Müller, M. T. Pope), KLUWER, Dordrecht, Netherlands, NATO Science Series II, Vol. 98, 2003. (d) D.-L. Long, E. Burkholder and L. Cronin, *Chem. Soc. Rev*., 2007, **36**, 105. (e) A. Dolbecq, E. Dumas, C. R. Mayer and P. Mialane, *Chem. Rev*., 2010, **110**, 6009. (f) U. Kortz, A. Müller, J. V. Salgeren, J. Schnack, N. S. Dalal and M. Dressel, *Coord. Chem. Rev*., 2009, **253**, 2315. (g) P. Gouzerh and A. Proust, *Chem. Rev*., 1998, **98**, 77. (h) D.-L. Long, R. Tsunashima and L. Cronin, *Angew. Chem. Int. Ed*., 2010, **49**, 1736.

10 (a) T. Yamase, *Chem. Rev.*, 1998, **98**, 307. (b) L. Yang, Z. Zhou, P. Ma, J. Wang and J. Niu, *Cryst. Growth Des.*, 2013, **13**, 2540. (c) Y. Wang, P. Ma and J. Niu, *Dalton Trans.*, 2015, **44**, 4679. (d) Y. Chen, G. Yu, F. Li, C. Xie and G. Tian, *J. Mater. Chem. C.*, 2013, **1**, 3842. (e) X. Luo and C. Yang, *Phys. Chem. Chem. Phys.*, 2011, **13**, 7892. (f) K. Hakouk, O. Oms, A. Dolbecq, H. El Moll, J. Marrot, M. Evain, F. Molton, C. Duboc, P. Deniard, S. Jobic, P. Mialane and R. Dessapt, *Inorg. Chem*., 2013, **52**, 555. (g) R. Dessapt, M. Collet, V. Coué, M. Bujoli-Doeuff, S. Jobic, C. Lee and M.-H. Whangbo, *Inorg. Chem.*, 2009, **48**, 574.

11 (a) S. Liu, D. G. Kurth, H. Möhwald and D. Volkmer, *Adv. Mater*., 2002, **14**, 225. (b) G. Gao, L. Xu, W. Wang, W. An, Y. Qiu, Z. Wang and E. Wang, *J. Phys. Chem. B*, 2005, **109**, 8948. (c) L. Jin, Y. Fang, P. Hu, Y. Zhai, E. Wang and S. Dong, *Chem. Commun*., 2012, **48**, 2101.

12 (a) L. Xu, E. Wang, Z. Li, D. G. Kurth, X. Du, H. Zhang and C. Qin, *New J. Chem*., 2002, **26**, 782. (b) J.-D. Compain, P. Mialane, A. Dolbecq, J. Marrot, A. Proust, K. Nakatani, P. Yu and F. Sécheresse, *Inorg. Chem*., 2009, **48**, 6222.

13 (a) L. Xu, H. Zhang, E. Wang, D. G. Kurth, and Z. Li, *J. Mater Chem*., 2002, **12**, 654. (b) H. Li, W. Qi, W. Li, H. Sun, W. Bu and L. Wu, *Adv. Mater*., 2005, **17**, 2688.

14 A. Parrot, G. Izzet, L.-M. Chamoreau, A. Proust, O. Oms, A. Dolbecq, K. Hakouk, H. El Bekkachi, P. Deniard, R. Dessapt and P. Mialane, *Inorg. Chem*., 2013, **52**, 11156.

RSC Advances Accepted Manuscript

This journal is © The Royal Society of Chemistry [year]

15 O. Oms, K. Hakouk, R. Dessapt, P. Deniard, S. Jobic, A. Dolbecq, T. Palacin, L. Nadjo, B. Keita, J. Marrot and P. Mialane, *Chem. Commun.*, 2012, **48**, 12103.
16 A. Saad, O. Oms, J. Marrot, A. Dolbecq, K. Hakouk, H. El Bekkachi, S. Jobic, P. Deniard, R. Dessapt, D. Garrot, K. Boukheddaden, R. Liu, G. Zhang, B. Keita and P. Mialane, *J. Mater. Chem. C*, 2014, **2**, 4748.
17 (a) K. Hakouk, O. Oms, A. Dolbecq, J. Marrot, A. Saad, P. Mialane, H. El Bekkachi, S. Jobic, P. Deniard and R. Dessapt, *J. Mater. Chem. C*, 2014, **2**, 1628. (b) J.-D. Compain, P. Deniard, R. Dessapt, A. Dolbecq, O. Oms, F. Sécheresse, J. Marrot and P. Mialane, *Chem. Commun*., 2010, **46**, 7733. (c) J.-D. Compain, P. Mialane, J. Marrot, F. Sécheresse, W. Zhu, E. Oldfield and A. Dolbecq, *Chem. Eur. J.*, 2010, **16**, 13441.
18 J. Li, *J. Clust. Sci.*, 2002, **13**, 137.
19 D. Hagrman, P. J. Hagrman and J. Zubieta, *Angew. Chem., Int*., 1999, **38**, 3165.
20 R. Klajn, *Chem. Soc. Rev*. 2014, **43**, 148.
21 P. Mialane, G. J. Zhang, I. M. Mbomekallé, P. Yu, J. -D. Compain, A. Dolbecq, J. Marrot, F. Sécheresse, B. Keita and L. Nadjo, *Chem. Eur. J*., 2010, **16**, 5572.
22 S. Benard and P. Yu, *Chem. Commun*. 2000, 65.
23 C. Sanchez, J. Livage, J. P. Launay, M. Fournier, *J. Am. Chem. Soc.* 1983, **105**, 6817.
24 W. G. Klemperer, *Inorg. Synth.*, 1990, **27**, 74.
25 G. M. Sheldrick, SADABS; program for scaling and correction of area detector data, University of Göttingen, Germany, 1997.
26 R. Blessing, *Acta Crystallogr.*, 1995, **A51**, 33.
27 G. M. Sheldrick, SHELX-TL version 5.03, Software Package for the Crystal Structure Determination, Siemens Analytical X-ray Instrument Division : Madison, WI USA, 1994.
28 P. Kubelka and F. Munk, *Z. Techn. Physik*, 1931, **12**, 593.

RSC Advances Accepted Manuscript